Supporting Information

In-situ Forming Thermally Shrinkable Electrospun Nanofiber Membranes for Wound Healing

Tianci Sun,†[a] Xu Yan,†[a] Bin Xia,†[a] Xiaofei Shen,†[a] Weiwei Fang,[a] Wanchuan Xu,[a] Zihui Fan,[a] Yunfeng Yao,[a] Longxiang Tang,[a] Yunjun Xu,[b] Lei Xia,[a] Qing Li,[c] Xiaopeng Ma,[d] Rende Ning,[e] and Tao He*[a]

[a]School of Chemistry and Chemical Engineering, Anhui Province Key Laboratory of Value-Added Catalytic Conversion and Reaction Engineering, Anhui Province Engineering Research Center of Flexible and Intelligent Material, Hefei University of Technology, Hefei, Anhui 230009, P. R. China.

[b]Department of Radiology. The First Affiliated Hospital of USTC University of Science and Technology of China, Hefei, Anhui 230036, P. R. China.

[c]Department of Laboratory Medicine, The First Affiliated Hospital of USTC, Division of Life Sciences and Medicine, University of Science and Technology of China. Hefei, 230001, P.R. China.

[d]Department of General Surgery, The First Affiliated Hospital of USTC, Division of Life Science and Medicine, University of Science and Technology of China, No.17, Lu Jiang Road, Hefei, Anhui Province 230001, P. R. China.

[e]The Third Affiliated Hospital of Anhui Medical University, The First People's Hospital of Hefei, Anhui, Hefei 230000, P. R. China.

Materials and Methods

Materials.

All chemicals were purchased without further purifications unless noted elsewhere. N-butyl methacrylate (nBMA) was purified by neutralized aluminum oxide column before using for polymerization. N-Isopropyl acrylamide (NIPAM) was purified by recrystallization from n-hexane. All animals experiments were approved by the ethics committee of Anhui Medical University and sacrificed the ethical standards for laboratory animals (LLSC20242233).

Characterizations.

The nuclear magnetic resonance (NMR) spectra of the polymers were recorded using an Agilent VNMRS 600 superconducting NMR spectrometer. Deuterated dimethyl sulfoxide (DMSO-d6) was used as the solvent for sample dissolution during measurement. The number-average molecular weight (Mn) and dispersity (Đ) of the polymers were determined by gel permeation chromatography (GPC) using a Waters 1515-2414 system under standardized conditions: a temperature of 35 °C, tetrahydrofuran (THF) as the mobile phase, and a flow rate of 1.0 mL/min.

Synthesis of PNB polymer.

The synthetic scheme of the PNB polymer was shown in Figure S1. Typically, under a nitrogen atmosphere, 4-cyano-4-(phenylcarbonylthio)valeric acid (CTA, 0.0164 g, 0.058 mmol), N-isopropylacrylamide (NIPAM, 2.00 g, 17.67 mmol), acryloyl-N-succinimide (NSA, 0.0997 g, 0.5891 mmol), and 5.0 mL of 1,4-dioxane were added to a 25 mL polymerization flask and completely dissolved. Subsequently, n-butyl methacrylate (n-BMA, 0.6702 g, 4.713 mmol) and azobisisobutyronitrile (AIBN, 4.83 mg, 0.029 mmol) were introduced into the solution. After dissolution, the reaction mixture was subjected to three freeze-pump-thaw cycles using liquid nitrogen to remove dissolved oxygen. The solution was then polymerized at 78 °C in an oil bath for 8 h. After the reaction was completed, the resulting polymer was precipitated in n-hexane three times, followed by vacuum drying overnight to yield the triblock copolymer P(NIPAM-nBMA-NSA). The product P(NIPAM-nBMA-NSA) was characterized by ^{1}H-NMR and GPC, and the data are presented in Figure S2a and S2c.

In a subsequent step, the obtained P(NIPAM-nBMA-NSA) (2.00 g, 0.0467 mmol), dopamine hydrochloride (94.5 mg, 0.9345 mmol), and triethylamine (0.0886 g, 0.467 mmol) were dissolved in 10.0 mL of dichloromethane. Under a nitrogen atmosphere, the solution underwent three additional freeze-pump-thaw cycles to ensure oxygen exclusion. The mixture was then stirred at room temperature for 16 h. After reaction completion, the product was precipitated in n-hexane three times and dried under vacuum overnight to afford the final functional copolymer P(NIPAM-co-nBMA-

DOPA) (abbreviated as PNB). The product PNB was characterized by ^{1}H-NMR (Figure S2b).

Preparation of electrospinning precursor solutions with different ZnO concentrations.

1.0 g of PNB was dissolved in 3.0 mL of anhydrous ethanol and stirred continuously until a homogeneous solution. Subsequently, ZnO at mass fractions of 0%, 1%, 2%, and 4% was added to the PNB solution, and the mixtures was stirred at room temperature for 2 h to prepare four electrospinning precursor solutions respectively. These solutions are designated as PNB, $PNBZ_1$, $PNBZ_2$, and $PNBZ_4$, respectively.

Preparation of electrospun nanofiber membranes with different ZnO concentrations.

2 mL of the precursor solution was added into a syringe and mounted onto a portable electrospinning device. The distance between the nanofiber collector and the needle tip should be maintained at 8-10 cm. The power switch was active to allow the spinning solution to slowly extrude from the needle tip and form a stable Taylor cone. During droplet elongation, the application of a high-voltage electric field induced fiber formation through electrostatic stretching, resulting in the deposition of nanofibers onto the collector and the subsequent formation of electrospun fibrous membranes. The electrospinning parameters were as follows: a polymer concentration of 20-40 wt%, a syringe volume of 5 mL, a working distance of 10 cm, an applied voltage of 18 kV, and a feed rate of 3 mL/h. The environmental humidity was controlled between 30% and 60%, and the ambient temperature was maintained at room temperature (25°C).

Characterizations of electrospun nanofiber membranes.

The electrospun nanofiber membranes were characterized using X-ray photoelectron spectroscopy (XPS) and X-ray diffraction (XRD). The morphology of electrospun nanofiber membranes was characterized by scanning electron microscopy (SEM). Fiber diameters were analyzed using ImageJ software, with 200 randomly selected fibers measured to determine diameter distribution through statistical analysis.

Dynamic Mechanical Analysis (DMA) of electrospun nanofiber membranes.

We prepared $PNBZ_4$ membranes with dimensions of 50 mm (length) × 1 mm (width) × 0.2 mm (thickness) for DMA testing using a NETZSCH GABO EPLEXOR 500N instrument. The tests were performed at a frequency of 10 Hz over a temperature range of 0 to 50°C.

Water contact angle test of electrospun nanofiber membranes.

To evaluate the surface wettability of electrospun nanofiber membranes, the contact angles were measured using a contact angle analyzer (CA700, China). Each measurement was performed in triplicate to ensure reproducibility.

Evaluation of the water vapor transmission rate of electrospun nanofiber membranes.

To evaluate the air permeability of electrospun nanofiber membranes, the water vapor transmission rate (WVTR) was determined in accordance with the ASTM E96/E96M standard. Briefly, 9 mL of 0.01 M phosphate-buffered saline (PBS) was placed into 10 mL centrifuge tubes, and medical dressings (MD), medical gauze (MG), PNB, PNBZ1, PNBZ2, and PNBZ4 membranes were individually sealed over the tube openings. The

effective diffusion area of each tube opening was measured and recorded as S, and the initial mass of each tube was recorded as W_0. The tubes were then incubated in a controlled environment chamber at 37°C and 60% relative humidity for 24 h, after which the final mass was measured and recorded as W_2. Each experimental group was tested in triplicate. The WVTR was calculated using the following equation:

$$\text{WVTR}(g/m^2 \cdot 24h) = \frac{W_2 - W_0}{S} * 100$$

Evaluation of the water absorption capacity of electrospun nanofiber membranes.

To evaluate the wound exudate absorption capacity of electrospun nanofiber membranes, the water absorption capacity was measured as follows. The initial weight of each dressing (W_0) was measured, after which the samples were immersed in phosphate-buffered saline (PBS) at room temperature for 24 h. Subsequently, the hydrated dressings were gently transferred to a Petri dish and allowed to stand for 1 minute to remove excess surface liquid. The dressings were then reweighed, and the final weight was recorded as W_1. The water absorption capacity was calculated using the following formula:

$$\text{Water Uptake Rate} = \frac{W_1 - W_0}{W_0} * 100$$

Thermal shrinkage behavior evaluation of electrospun nanofiber membranes.

To evaluate the temperature responsiveness of electrospun nanofiber membranes, thermal shrinkage tests were performed in a thermostatically controlled water bath at 37 °C. The membranes were uniformly cut into circular specimens with a diameter of

2 cm. The remaining area of the samples was measured at predetermined time intervals. The thermal shrinkage ratio was calculated according to the formula St/S0, where S0 and St denote the initial area of the membrane samples and their area at time t, respectively. At least three replicates were tested per experiment to ensure statistical reliability.

Adhesion performance evaluation of electrospun nanofiber membranes.

To evaluate the adhesion performance of electrospun nanofiber membranes, the following procedures were applied. Porcine skin samples were cut into 50 mm × 50 mm sections and thoroughly degreased prior to use. The nanofibers were then fabricated via in situ electrospinning directly onto the surface of the porcine skin, with the dermal side securely fixed using adhesive. Subsequently, adhesion strength was measured using an electronic universal material testing machine. Additionally, electrospun nanofiber membranes were deposited *in situ* onto human finger joints, and their adhesive performance was assessed by flexing the fingers at various angles to observe resistance to delamination.

Two pieces of porcine skin, each measuring 100 cm in length, 1.5 cm in width, and 2 mm in thickness, were individually clamped in a universal testing machine (INSTRON 6800). The $PNBZ_4$ membrane was then adhered between the two pieces of porcine skin. Subsequently, the membrane was heated to 37°C, and the change in shrink force was recorded.

***In vitro* antibacterial evaluation of electrospun nanofiber membranes.**

The *in vitro* antibacterial performance of the electrospun nanofiber membranes was evaluated using Escherichia coli (E. coli) and methicillin-resistant Staphylococcus aureus (MRSA). $PNBZ_1$, $PNBZ_2$, and $PNBZ_4$ membranes were cut into discs with a diameter of 2 cm, sterilized, and placed on solid agar media inoculated with E. coli and MRSA, respectively, followed by incubation at 37 °C for 24 hours. The size of the inhibition zones formed around the membranes was observed and measured, with each group tested in triplicate.

Evaluation of cytotoxicity and biocompatibility of electrospun nanofiber membranes.

MTT assay and calcein-AM/PI staining were employed for cytotoxicity assessment. Briefly, NIH-3T3 cells were seeded into 96-well plates and incubated at 37 °C in a humidified atmosphere containing 5% CO_2 for 24 h. Subsequently, $PNBZ_4$ membranes and 100 μL of culture medium were added to each well and further incubated for an additional 24 hours. After removal of the supernatant, 20 μL of MTT solution (5 mg/mL) was added to each well and incubated for 4 h. The formazan crystals were then dissolved by adding 200 μL of dimethyl sulfoxide (DMSO), and the absorbance was measured at 450 nm. In parallel, NIH-3T3 cells co-cultured with $PNBZ_4$ membranes were stained with calcein-acetoxymethyl/propidium iodide (calcein-AM/PI) for 15 minutes, and live/dead cell distribution was observed and imaged under a fluorescence inverted microscope.

The hemolytic potential of the $PNBZ_4$ membrane was evaluated using mouse blood samples (n = 5). Normal saline served as the negative control, and deionized water as

the positive control. The $PNBZ_4$ membrane was placed in a centrifuge tube containing anticoagulated mouse blood and centrifuged at 3000 rpm for 5 minutes. The supernatant was then collected, and its absorbance was measured at 545 nm to assess the extent of hemolysis induced by the membrane.

***In vivo* evaluation of wound closure efficacy mediated by thermal shrinkage of electrospun nanofiber membranes.**

The thermal shrinkage capability of the $PNBZ_4$ membrane was evaluated using a full-thickness mouse skin incision model to assess its in vivo wound closure efficacy. Female ICR mice (25–30 g) were used in this study. All animals were anesthetized using an anesthesia machine, and the dorsal hair was shaved and disinfected with iodine. Two distinct types of full-thickness wounds were created along the midline of the back: one was a linear incision measuring 20 mm in length, and the other was a circular wound with a diameter of 10 mm. Mice were randomly assigned to two groups according to wound type. The control group received standard medical dressings (MD), while the experimental group was treated with $PNBZ_4$ membranes fabricated via in situ electrospinning to ensure complete wound coverage. After 24 h, the dressings were gently removed, and wound widths were recorded. The degree of wound contraction was evaluated to assess the applicability of the membrane for wounds involving significant tissue loss.

***In vivo* evaluation of electrospun nanofiber membranes for promoting wound healing in a murine model of *MRSA*-infected skin wounds.**

To further investigate the effect of the $PNBZ_4$ membrane on the healing of severely infected wounds, a rat model of *MRSA*-infected skin wounds was established. Sprague-Dawley rats (SPF grade) were used in the study and randomly assigned to three groups (n = 7): control group, PNB membrane group, and $PNBZ_4$ membrane group. Briefly, the rats were anesthetized, dorsal hair was shaved, and the skin was disinfected with iodine. A full-thickness circular wound measuring 10 mm in diameter was created on the dorsum of each rat. Subsequently, 100 μL of *MRSA* suspension at a concentration of 10^6 CFU/mL was inoculated onto the wound site and allowed to establish infection for 2 hours. In the control group, wounds were treated with medical dressings (MD), whereas in the PNB and PNBZ4 membrane groups, membranes were fabricated directly at the wound site via *in situ* electrospinning for 3 minutes to ensure complete coverage. Wound healing progression was monitored by regular photographic documentation. The wound healing rate was calculated using the following formula:

$$\text{Wound healing rate}\ (\%) = \frac{W_0 - W_n}{W_0} * 100$$

Among them, Wn represents the wound area on days 2, 4, 6, 8, 10, 12, and 14.

To further evaluate the wound healing process in *MRSA*-infected wounds across different treatment groups, rats were euthanized on days 4, 8, and 14 post-treatment, and wound tissue samples were harvested for histopathological analysis using H&E and Masson's trichrome staining.

***In vivo* toxicity evaluation of electrospun nanofiber membranes.**

To evaluate the in vivo toxicity of $PNBZ_4$ membranes, *in situ* electrospinning was performed at the skin wound sites of healthy rats, with untreated rats serving as the

control group. All rats were euthanized 14 days post-treatment, and major organs (heart, liver, spleen, lung, and kidney) were harvested. The tissues were fixed in formalin and processed for H&E staining to assess potential histopathological alterations. Additionally, serum samples were collected from both the experimental and control groups on day 14 for comparative biochemical analysis to further evaluate the systemic toxicity of the $PNBZ_4$ membranes.

Statistical analysis.

The experimental data were analyzed using One-way ANOVA test followed by Dunnett's test. [statistical significance was considered when $p < 0.05$ (*), $p < 0.01$(**), $p < 0.001$(***)]. All error bars represented the standard deviations. All results were expressed as mean±SD.

Map Sum Spectrum	
Element	Wt. %
C	70.81
N	9.82
O	12.76
Zn	6.61
Total:	100.00

Table. S1 Quantitative analysis of ZnO dispersion of the $PNBZ_4$ membrane.

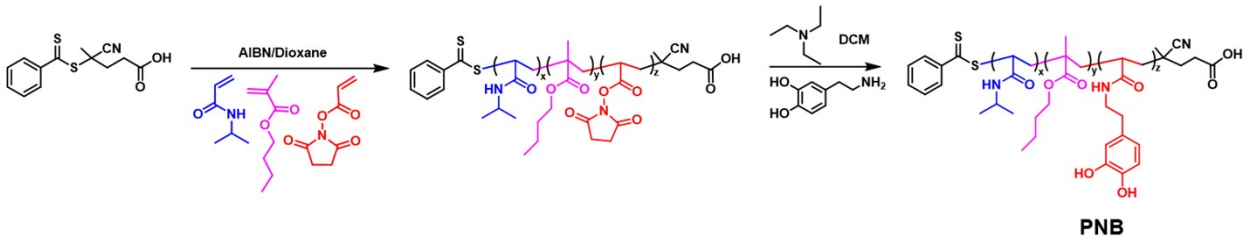

Fig. S1 Synthesis of ternary random copolymer of poly((N-isopropylacrylamide-co-nButyl Methacrylate-co-dopamine) (Poly(NIPAM-co-nBMA-DOPA), PNB), X, Y, Z represented 258, 41, 10 respectively.

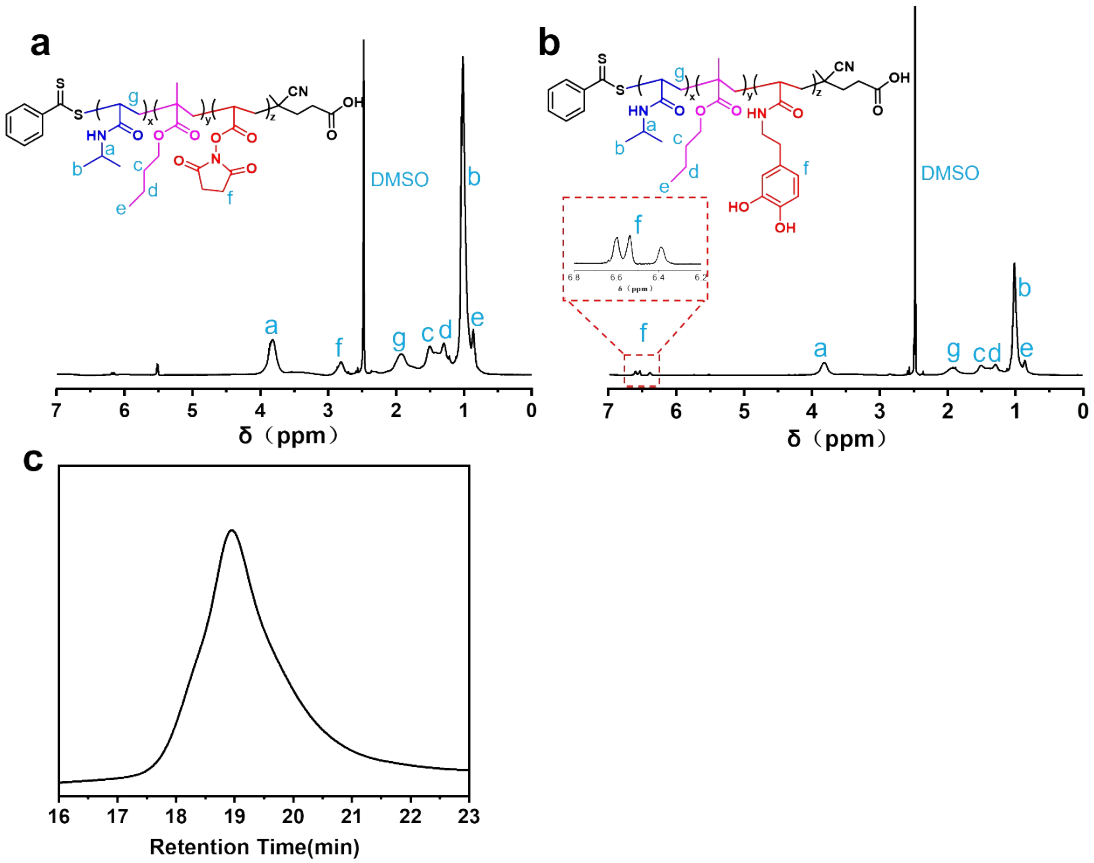

Fig. S2 [1]HNMR spectra of (a) P(NIPAM-nBMA-NSA) and (b) PNB. (c) GPC curve of P(NIPAM-nBMA-NSA) (M_n=38.1 kDa, PDI=1.16).

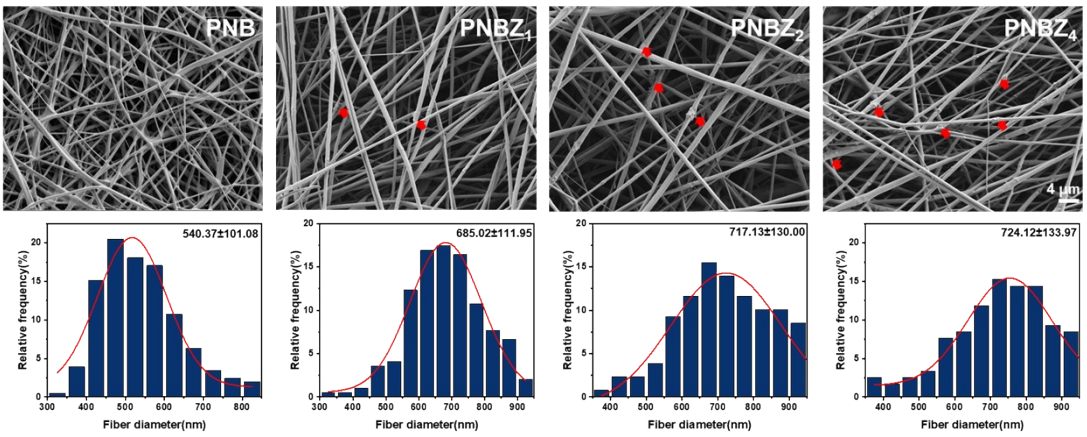

Fig. S3 Scanning electron microscopy images of the electrospun membranes and corresponding fiber diameter distribution histograms.

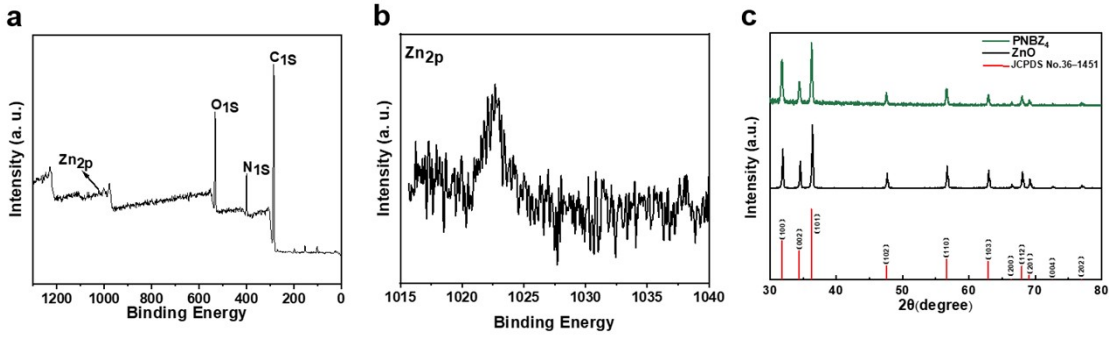

Fig. S4 (a), (b) XPS and (c) XRD spectra of the $PNBZ_4$ membrane.

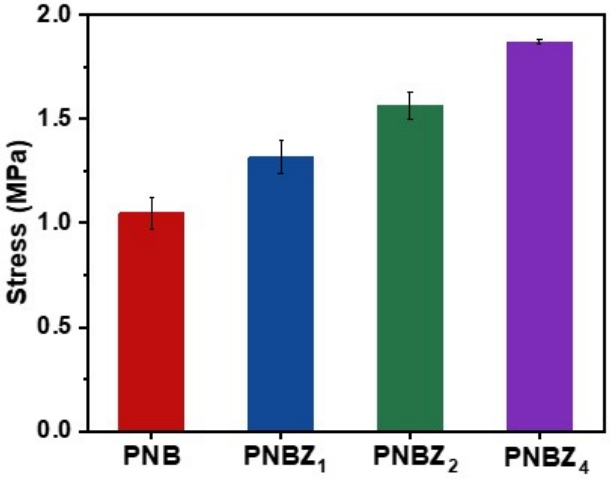

Fig. S5 Comparative analysis of Young's modulus for PNB, $PNBZ_1$, $PNBZ_2$, and $PNBZ_4$ membranes.

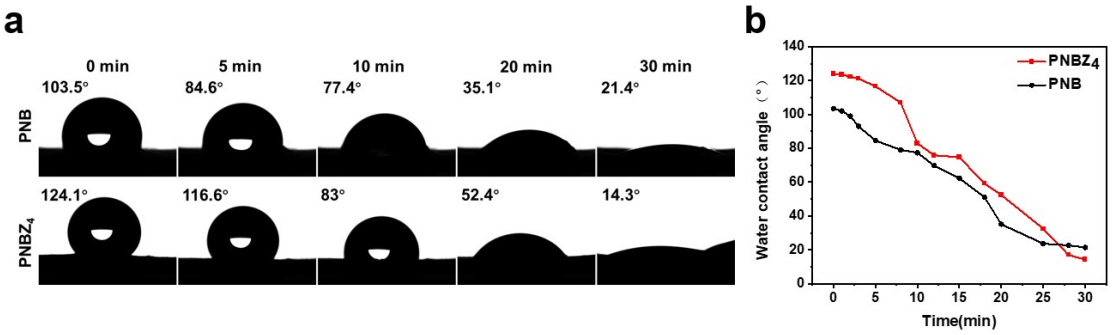

Fig. S6 Time-dependent contact angle measurements of the PNB and $PNBZ_4$ membranes, including (a) photographic documentation and (b) quantitative data profiles.

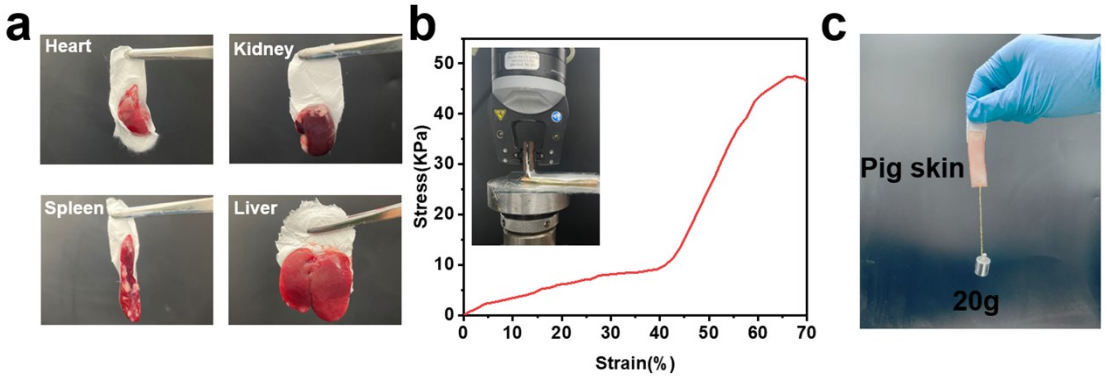

Fig. S7 (a) Images of the $PNBZ_4$ membranes adhering to rat organs, including the heart, liver, spleen, and kidney; (b) Adhesion force measurement curve and (c) load-bearing test images of the PNBZ4 membrane on fresh porcine skin

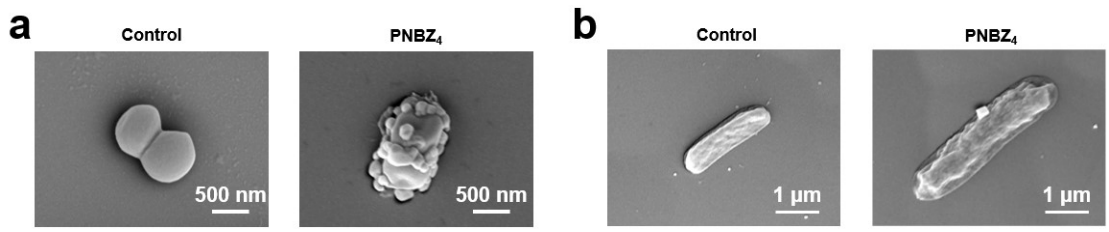

Fig. S8 SEM images with (a) *MRSA* and (b) *E. coli* treated by $PNBZ_4$.

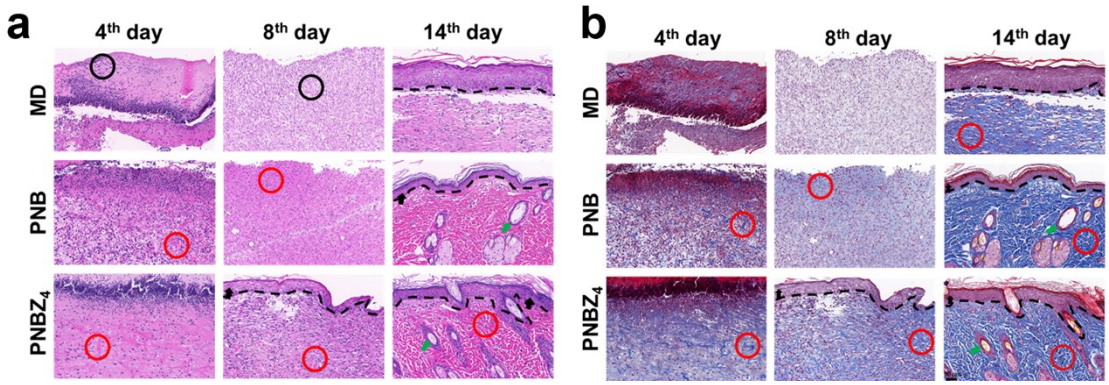

Fig. S9 Photomicrographs of skin tissue sections stained with (a) H&E and (b) Masson's trichrome at the wound site. Scale bar: 50 μm. Black circle, red circle, black arrow, green arrow, and black dashed line indicate inflammatory cells, collagen fibers, epidermis, hair follicles, and boundary of epithelium and dermis, respectively.

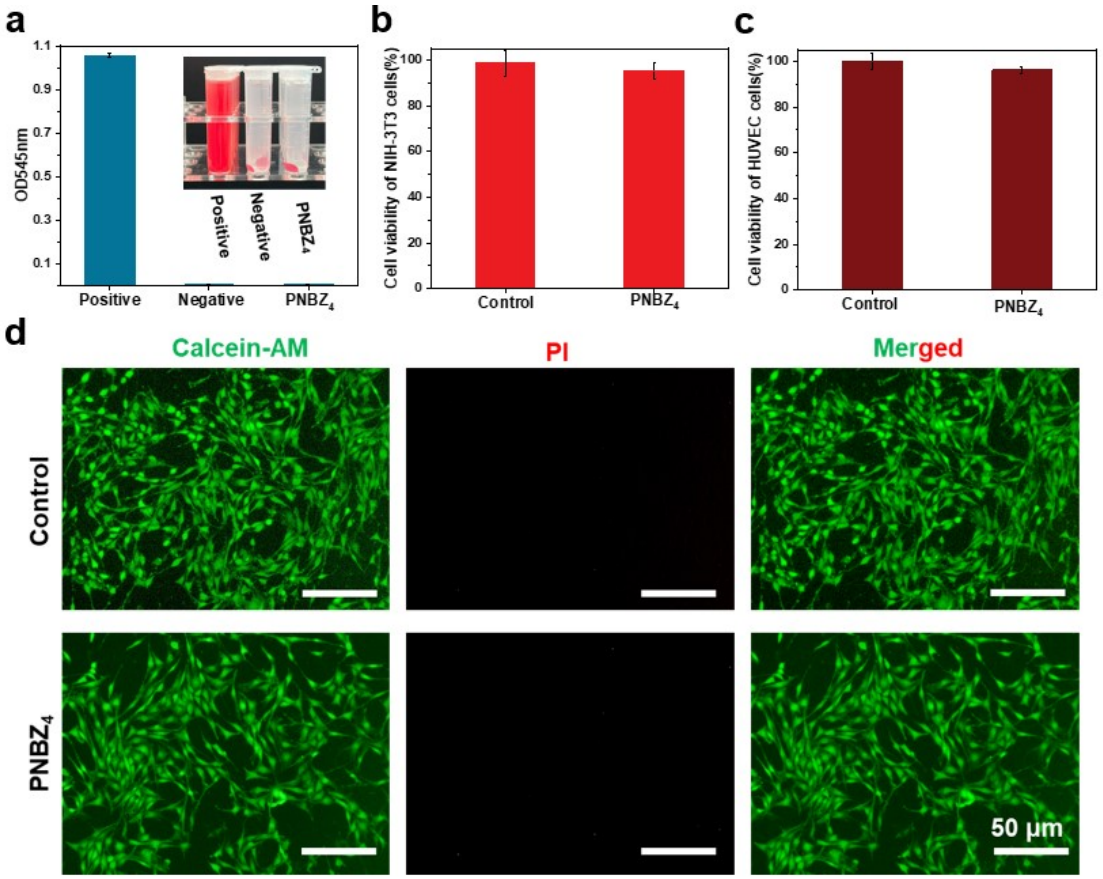

Fig. S10 (a) Hemolysis evaluation of $PNBZ_4$ membrane, n = 5. Cell toxicity evaluation of $PNBZ_4$ membrane on (b) NIH-3T3 mouse embryo fibroblast cells and (c) HUVEC cells. (d) Calcein acetoxymethyl ester (Calcein-AM)/propidium iodide (PI) staining of NIH-3T3 cells after exposed to $PNBZ_4$ membrane for 48 h. Scale bar, 50 μm.

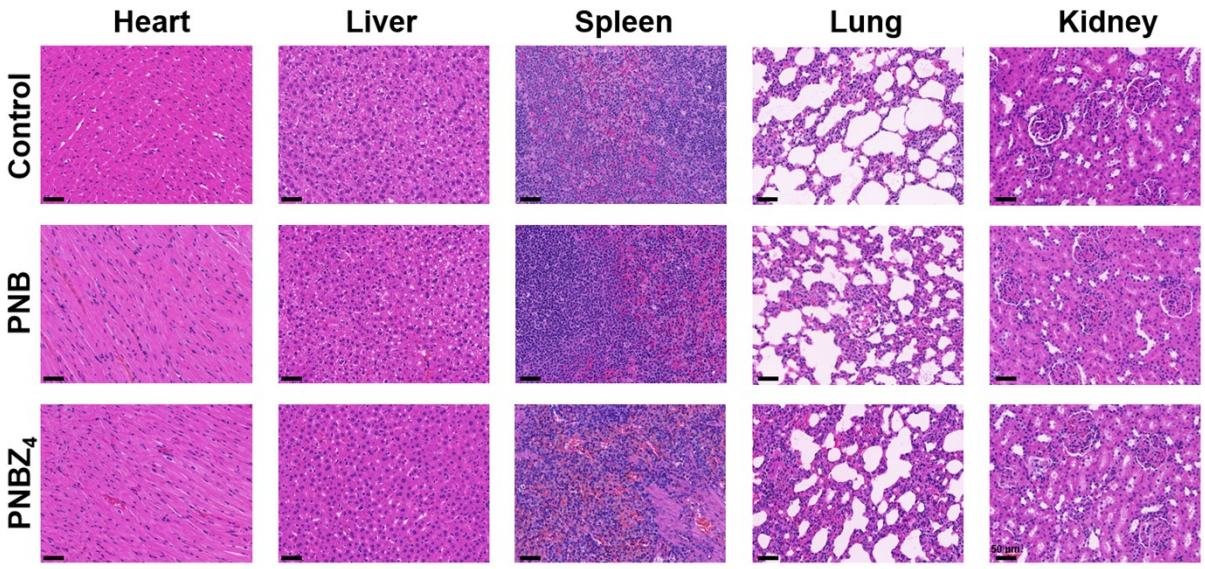

Fig. S11 H&E staining images of important organs (heart, liver, spleen, lung, and kidney) of rats implanted with PNB and $PNBZ_4$ membranes (scale bar = 50 μm).

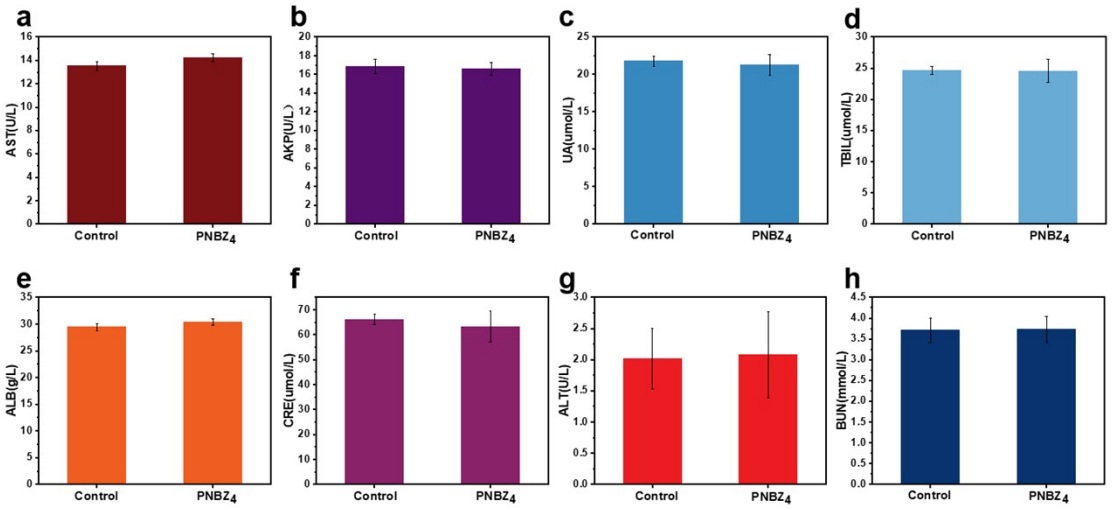

Fig. S12. Major blood biochemical values of control and after 14 days of $PNBZ_4$ membranes treatment in rats were measured, n = 5.

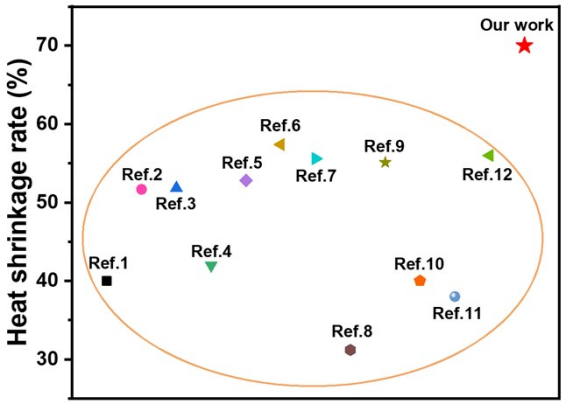

Fig. S13. Comparison of contraction efficiency between the electrospun membrane developed in this work and previously reported self-contracting hydrogels.

References:

1. H.Chen, R. Zhang, G. Zhang, X. Liang, C. Xu, Y. Li and F. J. Xu, *Advanced Materials,* 2024**,** **37**, 2410845.

2. J. Luo, Z. Liang, X. Zhao, S. Huang, Y. Gu, Z. Deng, J. Ye, X. Cai, Y. Han and B. Guo, *National Science Review,* 2025**, 12**, nwaf118.

3. Z. Lu, J. Cui, F. Liu, C. Liang, S. Feng, Y. Sun, W. Gao, Y. Guo, B. Zhang and W. Huang, *Advanced Healthcare Materials,* 2023**, 13**, 2303499.

4. Z. Bei, L. Ye, Q. Tong, Y. Ming, T. Yang, Y. Zhu, L. Zhang, X. Li, H. Deng, J. Liu, W. Chen, B. Chu and Z. Qian, *Cell Reports Physical Science,* 2024**, *5***.

5. Q.Zhong, R.Zhang, Y. Chen, S. Tan, L. Huang, J. Zhang and Z. Luo, *Advanced Functional Materials,* 2025, e12807.

6. M. Tian, J. Wan, X. Wang, J. Liu, M. Pan, H. Tan and Z. Pan, *Chemical Engineering Journal,* 2025, **514**, 163202.

7. Q. Cui, K. Zhang, X. Fei, C. Wang, S. Cheng, Y. Li and L. Xu, *European Polymer Journal,* 2025, **237**, 114178.

8. Q. Chen, S. Li, K. Li, W. Zhao and C. Zhao, *Advanced Science,* 2024**, 11**, 2306018.

9. Q. Xie, C. Yan, G. Liu, L. Bian and K. Zhang, *Advanced Materials,* 2024, **36**, 2406434.

10. Z. Ji, T. Wei, J. Zhu, J. Hu, Z. Xiao, B. Bai, X. Lv, Y. Miao, M. Chen, C. Wang, F. Pan, Y. Yang, M. Li and Q. Chen, *Nano Research,* 2024**, 17**, 7394-7403.

11. Y. Zhang, S. Wen, K. Zheng, X. Zhou, C. Huang, Y. Xu, J. Luo and G. Lu, *Biomacromolecules,* 2025, **26**, 5778-5790.

12. Q. Wang, W. Zheng, J. Wang, C. Jiao, D. Gao, J. Liu and B. Lu, *ACS Applied Materials & Interfaces,* 2025, **17**, 30747-30758.